Article

Polyclonal expansion of functional tumor-reactive lymphocytes infiltrating glioblastoma for personalized cell therapy

Martina Maffezzini[1,2,20], Silvia Musio [1,2,20], Natalia Di Ianni [1,2,20], Agnese Rumolo[3], Monica Patanè[4], Andrea Galluzzo[1,2], Irene Sambruni[1,2,5], Arianna Berlendis[2,6], Domenico Aquino[7], Giacomo Baso [2,8], Manuela Zingarelli[1,2,9], Manuel Facciolla[1,2], Luisa Maddaloni[2,6], Rossella Valentino[2,6], Rosina Paterra[2,6], Fabio Agistri[4], Mariangela Farinotti [2], Luca Mattei[10], Paola Coluccia[11], Francesco Acerbi[12,13], Francesco DiMeco[10,14,15], Bianca Pollo [4], Antonio Silvani[2], Marica Eoli[2,16], Catia Traversari[17,21], Daniela Montagna[3,18,19,21] & Serena Pellegatta [1,2,6,21] ✉

Tumor-infiltrating lymphocyte (TIL)-therapy has received FDA approval for the treatment of advanced melanoma and shows potential for broader applications in solid tumors, including glioblastoma. In this study, tumor-reactive TILs (tr-TILs) are isolated and enriched for CD137 expression from cavitron ultrasonic aspirator (CUSA) emulsions of 161 adult patients diagnosed with diffuse gliomas. Tr-TILs are successfully expanded in 87 out of the 161 patients, reflecting an expansion rate of 54%. Notably, the presence of IDH1 mutation and the cumulative dose of steroids are identified as significant negative predictors of expansion efficacy. The expanded tr-TILs exhibit distinct phenotypic and molecular dysfunctional features yet show upregulated expression of progenitor/memory-like markers and polyclonal T-cell receptors. Importantly, these tr-TILs demonstrate specific antitumor reactivity against autologous tumor cells in both in vitro and in vivo xenograft models. These findings provide a compelling background for a personalized immunotherapeutic approach while tackling one of the most significant challenges in oncology.

Cancer immunotherapy represents an appealing option for the treatment of glioblastoma, a devastating solid tumor for which radiotherapy and chemotherapy with temozolomide (TMZ) offer only limited efficacy[1], particularly in tumors where the unmethylated O-6-methylguanine-DNA methyltransferase (MGMT) promoter is associated with TMZ resistance and poor prognosis.

Using tumor-infiltrating lymphocytes (TILs), immune cells that naturally infiltrate a tumor, provides a simple and effective initial approach for developing personalized treatments. In adoptive cell therapy (ACT), TILs are extracted from a patient's tumor, expanded in

the laboratory, and then reintroduced into the patient to fight the cancer. Because TILs are specific to each individual's tumor, this method is considered personalized and relatively straightforward to implement compared to other advanced immunotherapy techniques[2].

TIL therapy has demonstrated clinical benefit, particularly in the setting of metastatic melanoma, and very recently, it was approved by the FDA as a drug for advanced melanoma[3].

The major advantage of TILs is their ability to recognize multiple antigens, including tumor-associated antigens, as well as a wide range of "unknown" neoepitopes and mutated proteins[4]. Over the years,

---

A full list of affiliations appears at the end of the paper. ✉e-mail: serena.pellegatta@istituto-besta.it

glioblastoma has been considered a cold tumor characterized by rare infiltrating T cells and a heterogeneous and highly immunosuppressive tumor microenvironment (TME), one of the most critical regulators of immune escape, inducing cancer therapeutic resistance and supporting the limited success of immunotherapeutic strategies[5,6]. Nevertheless, some independent studies have observed a local infiltration of T cells sustained by systemic immune responses during immune checkpoint blockade therapy. Particularly, immunotherapy strategies drive systemic expansion of effector tumor-specific T lymphocytes which migrate and infiltrate the tumor site, contributing to enhancing the local anti-tumor response. These findings support the notion that glioblastoma is not an irreversible cold tumor[7]. Notably, the development of novel and advanced technologies, such as single-cell RNA sequencing, has yielded unprecedented insights into tumor immune cell biology[8,9]. Transcriptome analyses demonstrated that glioblastoma progression and the composition of neoplastic cells are shaped by the reorganization of the immune microenvironment[10]. In glioblastoma many of the hampered networks involved in inflammation, immune cell chemotaxis and angiogenesis are active in the initial phases of the disease and remain active through recurrence[10]. Significant progress has recently been made in deciphering glioblastoma and TME heterogeneity through spatially resolved transcriptomics, metabolomics, and proteomics. Analysis of regionally shared transcriptional programs revealed spatial heterogeneity of immune infiltrates within specific "reactive-immune" regions, which are enriched in various myeloid cell subtypes and T cells, including memory and exhausted phenotypes[11]. Multiple molecular subtypes of myeloid cells have been identified within the TME, contributing to the heterogeneity in myeloid–T cell communication[11]. Additionally, tumor-associated myeloid cells and cytotoxic T lymphocytes are recruited and sequestered in hypoxic regions of glioblastoma, where they undergo reprogramming into an immunosuppressive phenotype[12].

Within TME, TILs engaged in tumor cell elimination become dysfunctional and are exhausted, expressing high levels of inhibitory checkpoints. This dysfunction is likely imprinted by strong immunosuppressive signaling in the TME, especially that mediated by regulatory myeloid cells[11,13]. However, most recently, it has been observed that glioblastoma is infiltrated by not exhausted T cells enriched in clonally expanded CD8^{+} effectors expressing GZMK, supporting the presence of an important T-cell subset within the tumor immune microenvironment with potential therapeutic implications[14].

In this study, we optimized a protocol for isolating and enriching TILs starting from CUSA material, which represents a large source of cancer cells as well as normal and immune cells. We select CD137, a costimulatory molecule expressed at high levels on activated non exhausted T cells in glioblastoma[15,16], as a specific marker for enriching tumor reactive infiltrating T (tr-TIL) cells. Polyclonal expanded tr-TILs exhibited a memory-like phenotype and a specific anti-tumor activity, supporting their therapeutic potential.

The basic concept behind this autologous ACT is harvesting T cells infiltrating glioblastoma, purifying the antigen-experienced tumor-reactive CD137^{+} TILs, expanding them to therapeutic numbers, and re-infusing them intratumorally or intraventricularly.

The transition of TIL therapy from research and experimental phases to clinical application in the near future holds significant promise for patients diagnosed with challenging-to-treat cancer types.

Results

CD137 is a specific marker for enriching tumor-reactive (tr-)TILs from gliomas
A total of 161 Cavitron Ultrasonic Surgical Aspiration (CUSA) materials from diffuse gliomas were collected and processed. The patients' clinical and molecular data, including IDH1 mutation status, MGMT status, and steroid dose, are reported in Table 1 and Supplementary Data 1.

CD137 was chosen as a specific marker for identifying tumor-reactive infiltrating lymphocytes (tr-TILs). Both CD8^{+} and CD4^{+} TILs isolated from CUSA material exhibited similar levels of CD137 expression, while matched peripheral blood mononuclear cells (PBMCs) displayed significantly lower levels of CD137. This expression pattern was consistent and uniform across all samples, including IDH1 wild-type and IDH1 mutant cases (Fig. 1a, b).

The magnetically enriched tr-TILs exhibited a high purity of CD137^{+} cells (Fig. 1b). The recovery of cells, including the total cell count and the proportions of CD45^{+}, CD8^{+}, and CD4^{+} T cells, was assessed both before and after immunoseparation, with a comparative analysis between IDH1 wild-type and IDH1 mutant samples (Fig. 1c–f, and Supplementary Data 2). When evaluated in vitro through co-culture with matched primary tumor cell lines, the CD137^{+} TILs demonstrated significant anti-tumor activity, revealed by increased IFNγ production compared to CD137- TILs (Fig. 1g).

The expression of CD137 was also assessed in other components of the TME present in the CUSA-derived material, including macrophages, monocytes, and neutrophils, and compared to that observed in enriched tr-TILs (Fig. 1h).

The expression of CD137 on tumor cells was evaluated using flow cytometry on 12 representative autologous primary cell lines growing in vitro as glioblastoma neurospheres (GB-NS), across all molecular subtypes. The analysis confirmed that mesenchymal GB-NS exhibited significantly higher levels of CD137 expression (Fig. 1i).

These findings were further supported by data from the GlioVis GBM database showing that transcription levels of TNFRSF9 gene, which encodes for CD137, are significantly elevated in glioblastoma samples compared to non-tumor tissue samples (Fig. 1j), and are markedly higher in the mesenchymal subtype compared with both classical and proneural subtypes (Fig. 1k). Notably, expression levels are similar in the unmethylated compared with the methylated samples (Fig. 1l), and significantly greater in IDH1 wild-type samples compared with those with IDH1 mutations (Fig. 1m). No significant differences in patient survival were found between high and low TNFRSF9 expression groups (Fig. 1n). However, among patients with methylated MGMT those with low TNFRSF9 had better survival than those with high TNFRSF9 (Fig. 1o). This survival advantage was not seen in patients with unmethylated MGMT (Fig. 1p).

The results obtained in the development phase confirmed that the optimized process for isolating T cells from CUSA material is suitable for obtaining high-purity tr-TILs for subsequent in vitro activation and expansion.

Tumor-reactive TILs are successfully expanded from a fraction of CUSA materials
An optimized process for in vitro activation and expansion was performed on CD137^{+} TILs purified from all 161 samples.

Tr-TILs were successfully expanded in 59% of the glioblastoma patients (81/138) and 26% of IDH1-mutant gliomas (6/23), whereas tr-TILs from the other patients did not expand beyond Day 14. The expansion rate ranged between 110- and 3600-fold (Supplementary Data 3). The median number of recovered TILs and the expansion rate were used as the cutoff for dividing patients into high-recovery-expanded ($> 5 \times 10^7$), low-moderate-expanded ($< 5 \times 10^7$, $> 5.8 \times 10^6$) and not expanded tr-TILs ($\leq 5.8 \times 10^6$) (Fig. 2a–c). The proliferation rate of the expanded tr-TILs increased exponentially between Day 14 and Day 18 (Fig. 2a, b).

An evaluation of the number of immune cells and the frequencies of CD45^{+}, CD4^{+}, CD8^{+}, and CD137^{+} cells before and after magnetic separation was performed by comparing the expanded and not expanded samples (Supplementary Data 3).

We then assessed the influence of tumor molecular characteristics and patient clinical parameters on the ability of tr-TILs to expand. Patients whose tr-TILs demonstrated no expansion had a significantly

Table 1 | Patient Characteristics

Number of cases	IDH-wt (*n* = 138)	IDH-mut (*n* = 23)						
		Astrocytoma (*n* = 14)			Oligodendroglioma (*n* = 6)		Recurrent GB (*n* = 3)	
		Grade 4 (*n* = 5)	Grade 3 (*n* = 8)	Grade 2 (*n* = 1)	Grade 3 (*n* = 4)	Grade 2 (*n* = 2)	Grade 4 (*n* = 2)	Grade 3 (*n* = 1)
Age (Mean ± SD)	60.7 ± 10.2	48.8 ± 10.2	42 ± 8.8	64	45.2 ± 22.8	46.5 ± 14.8	46.5 ± 4.9	39
Gender								
Male	100	5	2	1	2	2	2	1
Female	38	0	6	0	2	0	0	0
MGMT								
UnMet	94	2	3	0	0	0	1	0
Met	44	3	5	1	4	2	1	1
expanded	81	0	0	1	3	0	2	0
not expanded	57	5	8	0	1	2	0	1

IDH1 = Isocitrate dehydrogenase; *MGMT* = O-6-methylguanine-DNA methyltransferase; *n* = number.
The correlation between IDH1 mutation and expansion outcome is present in the corresponding source data.

longer mean duration of corticosteroid treatment (42.8 ± 25.2 days) compared to those with expanded tr-TILs (32.0 ± 20.3 days), corresponding to an approximate mean difference of 10 days (Fig. 2d). Additionally, the mean cumulative corticosteroid dose was higher in the not expanding tr-TIL group (263.3 ± 184.5 mg) compared to the expanding group (178.5 ± 115.2 mg), with a mean difference of 84.8 mg. However, no specific dosage cut-off was identified. (Fig. 2e, Supplementary Data 1). Considering only IDH1-mutant cases, the comparative analysis between expanded and not expanded samples did not reach statistical significance (Supplementary Fig. 1).

Notably, IDH1 mutation was associated with a negative expansion outcome (Table 1, *p* = 0.01; Chi-square test and Fisher's exact test). No other differences in pre-operative (i.e., tumor site; Supplementary Fig. 1) or molecular variables were found between the two groups.

Exhausted tr-TILs retain their progenitor memory status and exhibit polyclonal TCRs

The acquisition of memory and exhaustion phenotypes was assessed in CD137⁺ enriched T cells, both before and at the end of the in vitro expansion process.

According to the expression of memory markers (CD45RO and CCR7), before CD137 enrichment, both CD8⁺ and CD4⁺ TILs exhibited a mixture of T effector memory (Tem), T central memory (Tcm), and naïve or stem cell memory T cells (Tn/Tscm) (Supplementary Data 4, gating strategy in the Supplementary information section). A significantly higher percentage of Tcm was identified in both CD4⁺ and CD8⁺ T cell subsets within expanded and not expanded samples at the end of the culture period (Fig. 2f). The exhaustion phenotype was evaluated by quantifying the expression levels of LAG-3, TIM-3, and PD-1 on CD8⁺ and CD4⁺ T cells (Supplementary Data 5). A significantly higher percentage of TIM-3 positive cells was found in the CD4⁺ T cells of not expanded compared with expanded samples (Fig. 2g). The expression of TIM-3 by not expanded CD4⁺ TILs significantly correlates with the duration of steroid treatment (*p* = 0.04, *n* = 42, Spearman correlation; Source data).

The molecular characterization of 18 tr-TILs was performed over different time points during their expansion, from Day 7 to Day 18 for expanded samples and Day 14 for not expanded samples. Gene expression levels of *TCF7*, *PDCD1*, *HAVCR2*, *SELL*, *GZMK*, and *IFNG* were evaluated, identifying three distinct TIL subtypes based on their gene expression profiles (Fig. 2h–j).

T Progenitor Exhausted TILs (Tpex, *n* = 5) showed early and sustained expression of *TCF7*, *PDCD1*, and *GZMK*, with high memory gene expression (*SELL*) and low levels of *HAVCR2* and *IFNG* (Fig. 2h). T Intermediate Exhausted TILs (*n* = 7) were characterized by reduced

TCF7 and *GZMK* levels, showing increased *PDCD1* and *HAVCR2* expression, retained memory characteristics (*SELL*), and elevated *IFNG* levels, indicating a more differentiated state (Fig. 2i).

T Effector Exhausted TILs (*n* = 6) were identified by the loss of *TCF7* and *GZMK*, increased *PDCD1*, *HAVCR2*, and *IFNG* expression, indicating terminal differentiation while maintaining *SELL* expression similar to the intermediate subtype (Fig. 2j).

CD8⁺ T cell infiltration was assessed in 10 tumor specimens via immunohistochemistry (IHC), revealing a heterogeneous distribution pattern (Supplementary Fig. 2). The presence of tr-TILs was confirmed through dual staining for CD8 and CD137. CD8⁺ TILs expressing CD137 were localized within various regions of the TME, often in close proximity to vasculature (Fig. 3a–e). Some areas demonstrated high densities of CD8⁺ CD137⁺ T cells (Fig. 3b, c), whereas other regions contained CD8⁺ TILs lacking CD137 expression (Fig. 3d, e).

Furthermore, a population of CD8⁺ T cells expressing TCF1 was identified in the periphery, near the tumor-associated blood vessels, as confirmed by immunofluorescence analysis (Fig. 3f, g).

Next-generation *TCRVb* gene sequencing was performed on tr-TILs isolated and expanded from CUSA material of these 10 patients (Fig. 3h). Expanded tr-TILs from glioblastoma and recurrent glioblastoma preferentially expressed polyclonal TCRs. In contrast, among the not expanded samples, two tr-TILs originating from IDH1-mutated tumors showed restricted Vβ clonality.

A fully automated functional single-cell multiplexed secretome proteomics performed to define the polyfunctional state of TILs after their expansion, revealed a profile dominated by chemoattractive, effector, and stimulatory cytokine subsets (Supplementary Fig. 3).

These findings, encompassing the diversity of polyclonal TCRβ chain, the observed polyfunctionality, and the maintenance of progenitor cell status, collectively support the presence of a diverse T cell population within the TME, potentially capable of effectively mediating immune responses against tumor antigen heterogeneity.

Tumor-reactive TILs exhibit specific antitumor activity against autologous tumor cells

The antitumor activity of 12 tr-TIL was assessed against autologous GB-NS, belonging to proneural, mesenchymal, classical subtypes, in an in vitro co-culture system at 24, 48, and 72 h. Killing activity was evaluated by flow cytometry by measuring the residual tumor cells for the expression of B7-H3, a marker highly expressed on the majority of GB-NS[17]. In comparison to PBMCs obtained from three healthy donors, tr-TILs demonstrated significant antitumor activity within the first 24 h (Fig. 4a–c). The residual autologous tumor cells, assessed as absolute
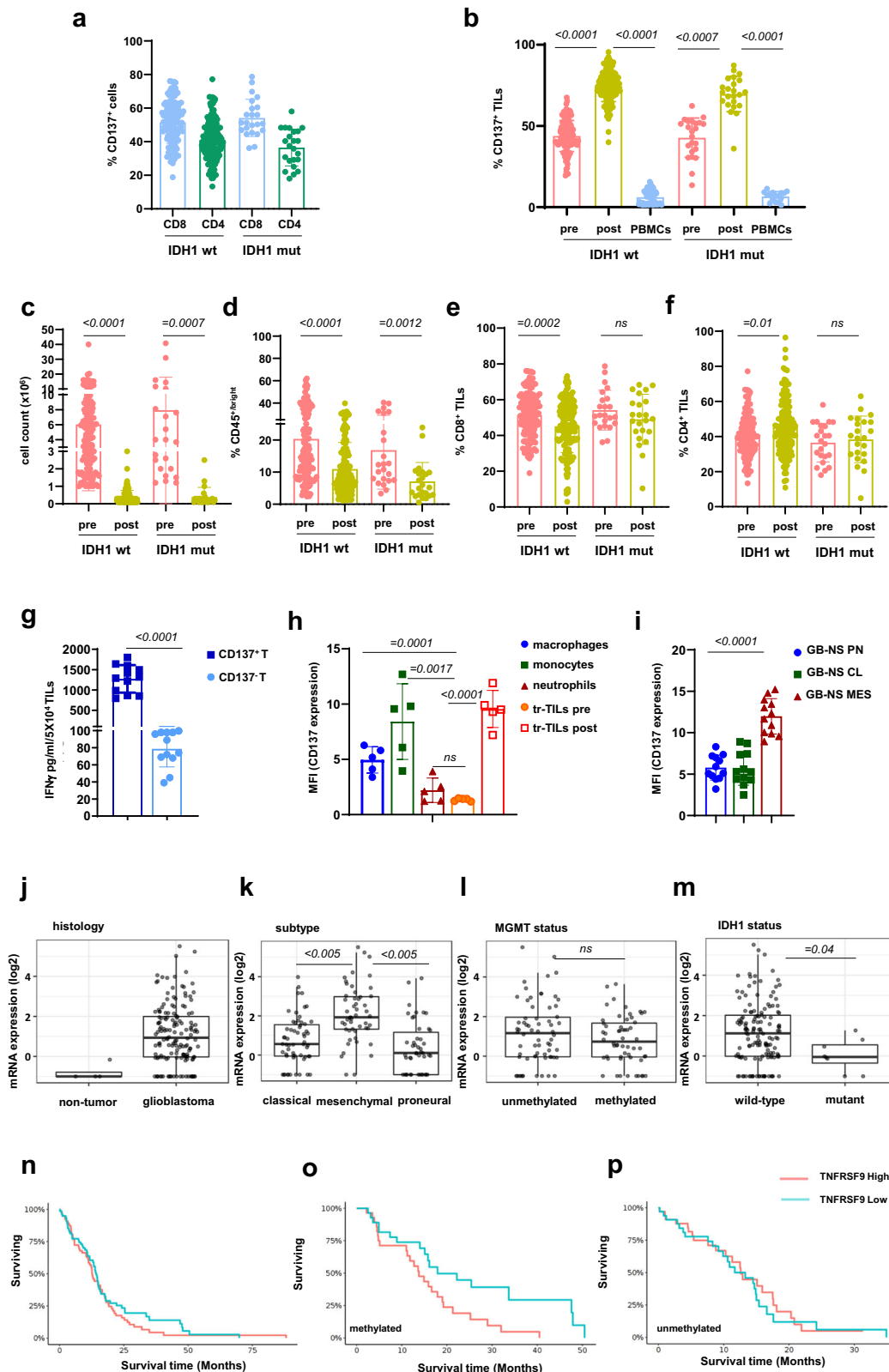
numbers, showed a significant decrease up to 72 h, regardless of their molecular subtype. In contrast, GB-NS continued to proliferate in the presence of donor PBMCs. Autologous patient PBMCs exhibited weak but detectable cytotoxic activity against the tumor cells. Evaluation of cytokine release in the supernatant recovered at 24 h revealed greater levels of the effector factor IFNγ in the presence of TILs than in the presence of PBMCs (Fig. 4d).

The potential tumor challenge was enhanced by extending the co-culture time to 5 days. Our analysis revealed that the upregulation of PD-L1 by GB-NS exhibited an inverse correlation with the release of IFNγ by tr-TILs. Specifically, GB-NS displayed peak PD-L1 expression levels on Days 3 and 5 of co-culture (Fig. 4e, f), which was associated with a progressive increase in the number of residual tumor cells, paralleling the decreased release of IFNγ by tr-TILs (Fig. 4g, h).

Fig. 1 | CD137+ tr-TILs are efficiently enriched from CUSA material. a–f Scatter plots with bars showing (**a**) the frequency of CD137 on CD8+ and CD4+ T cells after debris removal, and (**b**) on CD3+ T cells compared with matched PBMCs ($n = 161$ vs. $n = 77$), before and after CD137 enrichment; **c** the number of cells, and the percentage of (**d**) CD45+, (**e**, **f**) CD8+ and CD4+ T cells before and after CD137 enrichment ($n = 161$). Data are presented as mean ± SD and statistical significance was assessed using a two-tailed unpaired t test. **g** ELISA quantification of IFNγ secreted by CD137+ tr-TILs and CD137- TILs co-cultured with matched GB-NS at 24 h ($n = 12$, with 2 technical replicates averaged prior to statistical analysis using a two-tailed unpaired t test. **h** Bar histograms showing CD137 MFI of macrophages, monocytes, neutrophils and tr-TILs before (pre) and after (post) enrichment ($n = 5$) and (**i**) of GB-NS belonging to proneural, classical and mesenchymal molecular subtype ($n = 12$). Data are presented as mean ± SD and statistical significance was assessed using a two-tailed unpaired t-test. **j–m** CD137 mRNA expression levels in (**j**) glioblastoma samples compared with tumor-free brain samples ($n = 160$); **k** CD137 expression across glioblastoma molecular subtypes: proneural, classical, and mesenchymal ($n = 156$); **l**, **m** CD137 expression in glioblastoma stratified by (**l**) MGMT promoter methylation status ($n = 122$) and (**m**) IDH1 mutation status ($n = 150$). Box plots show median (center line), 25th and 75th percentiles (bounds of box), and minimum and maximum values (whiskers). Statistical differences were analyzed using Tukey's Honest Significant Difference (HSD) test. **n–p** Kaplan Meier curves of glioblastoma patients based on (**n**) the expression of TNFRSF9 (High TNFRSF9 [78 patients] vs. Low TNFRSF9 [77 patients]), **o** in MGMT met patients (High [28 patients] vs. Low [28 patients]), and (**p**) in MGMT unmet patients (High [33 patients] vs. Low [33 patients]); GlioVis dataportal; statistical significance between survival curves was assessed using the Log-rank (Mantel–Cox) test. Full numerical data and comprehensive details of statistical analyses are available in the corresponding source data tables for each figure. Source Data are provided as a Source Data file.

Blocking PD-L1 in vitro during the co-culture with αPD-L1 antibody significantly enhanced both the cytotoxicity against GB-NS and IFNγ production when compared to the isotype control (Fig. 4i–k). These findings support the notion that the upregulation of PD-L1 by GB-NS serves as an immune evasion mechanism and that PD-L1 blockade improves the responsiveness of tr-TILs, thereby reducing the number of residual tumor cells.

Overall, these results confirm the in vitro antitumor activity of the manufactured tr-TILs, thus supporting their use in T-cell therapy protocols.

Tumor-reactive TILs control glioma engraftment and progression in xenograft models

The functional activity of four TIL samples displaying differences in CD8+ and CD4+ T cells proportion was tested in xenograft models obtained by implanting autologous GB-NS intracranially into nude mice (Fig. 5a–d). Ten days after tumor implantation, tr-TILs and autologous PBMCs were infused using the same tumor coordinates (Fig. 5e). TIL doses ranged from 0.75×10^6 to 5×10^6, whereas PBMCs were administered only at the higher dose of 5×10^6. A cohort of tumor-bearing mice was left untreated as additional control (cTs) (Fig. 5f–i).

The infusion of 5×10^6 and 3×10^6 TILs improved survival in 70% and 60% of the treated mice, respectively. Tumor control was also achieved in mice treated with 1.5×10^6 TILs, with an improvement in 20–40% of the treated mice. Modest activity was also observed at the lowest dose, which prolonged survival by ~30 days compared with controls (Fig. 5f–i). In agreement with the in vitro data, autologous PBMCs showed a weak antitumor activity.

To better characterize the antitumor effect, the activation ability of T cells was assessed after exposure to matched GB-NS in vivo following intracranial infusion and in co-culture (Fig. 5j–m). The expression of the early activation marker CD69 on tr-TILs isolated from tumor masses was upregulated rapidly within 3 h and downregulated at 24 h, while CD137 was detected 6 h after TIL infusion, and its expression increased after 24 h. The number of TILs infused influenced both early and late activation (Fig. 5j–l). In in vitro co-culture CD69 showed an early increased expression, followed by a gradual but persistent CD137 upregulation (Fig. 5m).

Moreover, the effects of TIL therapy were monitored by 7 Tesla MRI performed on glioblastoma-bearing mice treated with 5×10^6 TILs (TIL 273) compared with controls. The tumor size quantification calculated from T2-weighted MRI images revealed a significantly smaller tumor volume in treated mice, supporting the anti-tumor activity of tr-TILs (Fig. 5n–p). Tumor progression and long-term TIL persistence were also documented by immunohistochemistry (IHC) analyses 60 days after treatment. Tumor cellularity and high extent of invasion were evident in control xenograft gliomas, whereas gliomas from treated mice were characterized by a peculiar distribution of tumor cells encapsulated in small and organized clusters to escape lymphocyte pressure (Fig. 6a, b).

Staining with a specific anti-CD3 human antibody revealed the presence of CD3+ T cells infiltrating the tumor mass. As expected, no CD3+ T cells were found within the tumor mass of the control mice (Fig. 6c, d). Notably, CD8-expressing TILs were detected within the tumor tissue but not in adjacent normal brain tissue (Fig. 6d inset).

Strong and homogeneous upregulation of PD-L1 was observed on the surface of tumor cells in treated, but not control, xenograft mice, supporting the functional activity of tr-TILs after intracranial administration (Fig. 6e, f). The secretion of IFNγ after interaction between TILs and tumor cells could upregulate PD-L1 expression, modulate the PD-1/PD-L1 axis, and contribute to TIL exhaustion. In control mice, GFAP+ astrocytic cells infiltrated the tumor mass, whereas in treated mice a GFAP-positive barrier surrounded tumor masses, contributing to their encapsulation and acting as a specific mechanism for evading TIL activity (Fig. 6g, h).

Potential long-term and off-target toxicities were evaluated. No behavioral or neurological abnormalities were observed after TIL infusion. Evaluation of weight loss (in % of the initial weight) was attributed to the tumor progression (Supplementary Fig. 4a). No detectable human CD45+ CD3+ cells were found in peripheral blood samples as early as 24 h, and as late as one week following TIL infusion (Supplementary Fig. 4b).

Taken together, these results demonstrated that autologous tr-TILs efficiently inhibited tumor growth in GB-bearing mice and that the number of TILs administered, and their activation status, were critical for antitumor efficacy.

A reliable and reproducible protocol is ready for the GMP-compliant transfer process

Developmental runs performed on a small scale were used to optimize the entire process (Supplementary Fig. 5a, b).

The protocol optimized for isolating and expanding tr-TILs from CUSA material and manufactured in non-GMP areas can be easily translated to GMP manufacturing, as the same GMP materials, commercially available clinical grade reagents, and the same type of equipment have been used. In addition, the product has been fully characterized by applying qualified or scientifically sound analytical methods. Supplementary Fig. 5 shows the entire process of tr-TIL manufacturing from the starting material to the final product.

Technology transfer included two important steps. The first involved the optimization of CD137+ TIL enrichment using the CliniMACS CD137-biotin GMP reagent. Phenotypic evaluation performed after magnetic selection revealed that the positive fraction was not enriched in CD137+ cells but that these cells were distributed in low percentages in both fractions, with a substantial loss of CD137+ cells (Supplementary Table 1). The non-GMP reagent has been incorporated
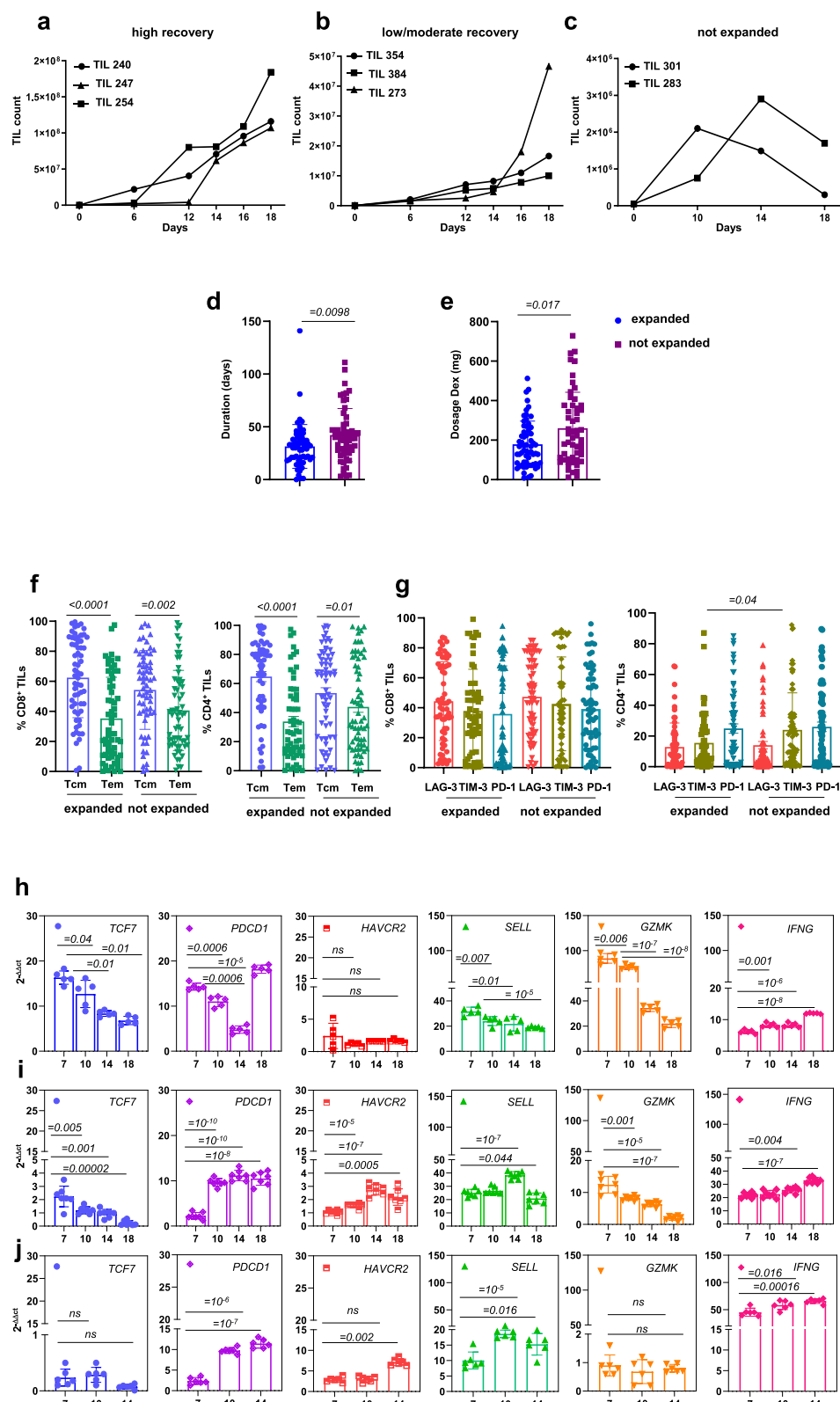
into our manufacturing process and subjected to appropriate validations.

A second rapid expansion was also investigated to improve the yield of TILs potentially available for treatment. An aliquot of tr-TILs frozen at the end of the culture was thawed and re-expanded for two weeks following the standardized expansion protocol (Supplementary Table 2). After expansion, the immunophenotype appeared stable,

supporting the possibility of introducing REP in the clinical process (Supplementary Fig. 6).

Discussion

The tremendous success of the use of TILs in advanced melanoma treatment, recently translated from FDA approval as a therapy[18], encouraged us to introduce this personalized approach in the clinical

Fig. 2 | tr-TILs retain memory status and express exhaustion markers.
a–**c** Representative proliferation kinetics of (**a**) expanded tr-TILs divided into high ($n = 3$), and (**b**) low-moderate recovery ($n = 3$), and (**c**) not expanded ($n = 3$).
d, **e** Scatter plot with bar graphs showing duration (**d**) and dosage (**e**) of steroid treatment with dexamethasone (dex) between expanded tr-TILs-patients ($n = 62$) vs. not expanded tr-TILs-patients ($n = 53$). Data are presented as mean ± SD, and statistical significance was assessed using a two-tailed Mann–Whitney test.
f, **g** Scatter plots with bars showing (**f**) central (Tcm) and effector (Tem) memory status of CD8+ and CD4+ TILs of expanded ($n = 71$) and not expanded ($n = 74$) samples at the end of expansion process (statistical significance was assessed using a two-tailed unpaired t test); (**g**) and exhaustion immunophenotype on CD8+, CD4+

tr-TILs for both expanded ($n = 72$) and not expanded ($n = 75$) tr-TILs at the end of expansion process. Data are presented as mean ± SD, and statistical significance was assessed using a two-tailed Mann–Whitney test. **h**–**j** Real-time PCR relative expression of genes related to (**h**) progenitor and (**i**) intermediate exhaustion status from Day 7 to Day 18 in expanded tr-TIL samples ($n = 5$ and 7 respectively, in blue in the supplementary tables), or related to (**j**) effector status in not expanded samples from Day 7 to Day 14 ($n = 6$, marked with an * in the supplementary tables). Data are presented as mean ± SD, with 2 technical replicates averaged prior to statistical analysis assessed using a two-tailed paired t-test. Full numerical data and comprehensive details of statistical analyses are available in the corresponding source data tables for each figure. Source Data are provided as a Source Data file.

treatment of rare but serious and untreatable cancers such as glioblastoma, thus addressing specific unmet medical needs.

The optimization of the process for isolating and expanding TILs from glioblastoma has several limitations. First, the low number and heterogeneous distribution of T cells within the tumor microenvironment can affect their isolation and enrichment for ex vivo expansion. Low levels of CD8+ TILs are scattered, isolated, and confined to perivascular spaces in newly diagnosed glioblastomas[19]. Preferentially excluded and located at the tumor periphery, CD8+ TILs presented an exhausted phenotype, retaining high expression levels of genes implicated in costimulatory pathways, including *TNFRSF4* (OX40) and *TNFRSF9* (41BB/CD137). Flow cytometry confirmed that CD8+ TILs expressing CD69 and CD103, and therefore displaying a T resident memory phenotype, were located exclusively at the tumor periphery[20].

Since small fragments of fresh tumor specimens cannot be representative of the TIL distribution within the entire mass, we decided to optimize T-cell isolation starting from the CUSA surgical emulsion, a powerful source of tumor material that we previously adopted as our reference system for primary glioblastoma cell lines[21]. Since the CUSA is used to remove the invasive margin of the tumor, it has two advantages: first, small tissue fragments are highly viable, unlike tissue from the tumor mass compromised by necrosis and apoptosis[22]; second, fragments can be more enriched in CD8+ T cells, considering their distribution at the tumor margin[19,23].

A potential limitation of the use of CUSA as a sonication system is that ultrasonic aspiration primarily destroys target cells and causes microhemorrhages. The system, in fact, does not discriminate between tumor cells or vessels, and as a result, the emulsion can also contain circulating blood-derived cells rather than real TILs. The identification of tumor-reactive TILs and their discrimination from bystander and blood-derived T cells were performed by evaluating the expression of the costimulatory molecule CD137, which is upregulated after the engagement between cancer cells and T cells. Previous evidence supports the upregulation of CD137 on TILs, preferentially on activated CD8+ T cells, or not exhausted CD8+ TILs[22]. Pichler and colleagues reported that CD137, which is expressed by exhausted TILs that retain effector memory characteristics, is essential for the presence and maintenance of CD8+ T cells within tumors[17]. CD137 signaling specifically promoted the proliferation and terminal differentiation of exhausted TILs even in the absence of active TCR signaling. However, combined treatment with a CD137 agonist and anti-PD-1 therapy can improve TIL function, inducing an antitumor response[24].

CD137 is expressed not only on activated T cells and NK cells, but also constitutively expressed at lower levels on monocytes, neutrophils, dendritic cells (DCs), endothelial cells[25,26] and astrocytes[26]. Many studies have documented CD137 expression in various malignancies, yet its biological significance remains unclear. It is hypothesized that CD137 may facilitate cancer cell proliferation and progression while inhibiting T cell activation[26,27]. CD137 on cancer cells may compete with CD137 on tr-TILs for binding to CD137L on antigen-presenting cells (APCs), potentially undermining anti-tumor immune responses[26]. In our study, we investigated the expression of *CD137* in glioblastoma by analyzing multiple patient datasets, correlating its

expression with the methylation status of MGMT and IDH1 mutation, and examining our primary cancer cell lines. The elevated *CD137* expression observed in mesenchymal tumors may be attributed to increased infiltration of CD137-positive immune cells. The high expression of CD137 on tumor cells did not affect the effector activity of tr-TILs during co-culture, suggesting that CD137 expression does not necessarily imply a role in immunosuppression. Furthermore, its function may vary depending on interactions with surrounding immune cells and the TME.

We have also confirmed that the immune cell components, including macrophages, monocytes, and neutrophils, present in the material after debris removal expressed CD137 on their surface.

Both CD8+ and CD4+ T cells expressing CD137 were efficiently enriched with high purity starting from the CUSA emulsion. These tr-TILs expressed variable levels of inhibitory receptors, including PD-1, TIM-3, and LAG-3, without affecting the feasibility of TIL expansion. Originally considered detrimental, T cell exhaustion is a functional adaptation enabling survival under persistent antigen stimulation and within an immunosuppressive TME[20,28]. Our in vitro and in vivo results support PD-1/PD-L1 axis as one of the potential tumor escapes exploited by glioblastoma cells to limit the TIL antitumor efficacy, which can be restored in combination with checkpoint inhibitors[29]. The expansion protocol was optimized and aimed at selecting and maintaining the memory-like features of isolated tumor-reactive TILs. IL-15, IL-7, and IL-21 were previously described as key cytokines influencing T-cell differentiation. IL-15 and IL-7 in combination have been shown to be involved in preserving minimally differentiated T cells during ex vivo expansion. Recently, it was demonstrated that IL-15 can induce the proliferation of exhausted T cells while retaining progenitor features rather than terminally differentiated subsets[30]. Furthermore, IL-21 has been shown to promote CD8+ memory T-cell longevity and prevent exhaustion[31]. Using this specific combination of cytokines, we observed efficient expansion in approximately half of the samples, obtaining a final product enriched in tr-TILs compatible with a memory-like phenotype.

Among the samples investigated from a molecular point of view, we observed a subgroup in which isolated and enriched tr-TILs expressed *TCF1/TCF7*, *SELL*, and *TOX*, supporting the presence of progenitor cells. The expression of *TCF1* was dynamically regulated during expansion, while the expression of *SELL*, encoding CD62L, was maintained until the end of expansion, confirming the presence of central memory T cells with important therapeutic implications. These observations, together with the evidence that exhausted TCF1+ CD8+ TILs were found at tumor borders[32], support the reliability of our process, corroborating that the CUSA system is an optimal option for isolating tr-TILs.

A critical limitation in the expansion ability was related to IDH1 mutation. Despite the limited number of samples harboring the mutation, the results allow us to state that the presence of the IDH1 mutation is critical for immune infiltration. As previously reported, IDH1 mutations can regulate the immune microenvironment in gliomas[33]. Specifically, IDH1-mutated gliomas were shown to be less effectively infiltrated by CD8+ T cells, which was attributed to the role
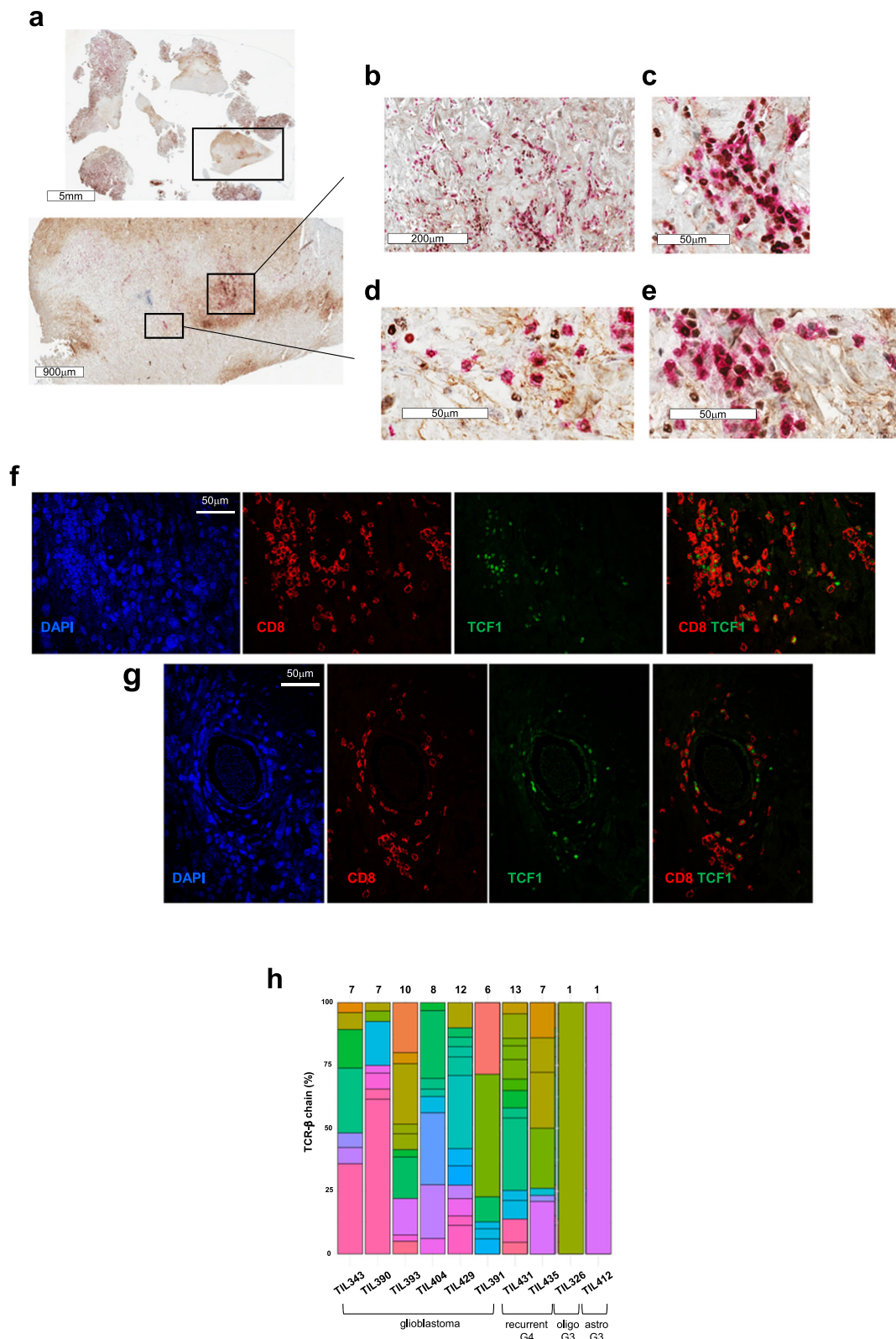
Fig. 3 | Expanded tr-TILs preserve tumor-specific T cell clonotypes and maintain progenitor status. a Entire tissue sections (upper panel- scale bar, 5 mm) and selected region (lower panel- scale bar, 900 μm) of a representative glioblastoma stained for CD8 (red) and CD137 (brown). **b, c** Two distinct areas showing CD8⁺ TILs co-expressing CD137 (scale bars, 200 μm and 50 μm), and (**d, e**) coexistence of CD8⁺ CD137⁺ TILs and CD8+ TILs lacking CD137 (scale bar, 50 μm). **f, g** Representative immunofluorescence images showing DAPI (blue), CD8 (red) and TCF1 (green) staining and CD8/TCF1 colocalization (merge) of (**f**) TIL 390 (scale bar, 50 μm) and (**g**) TIL 431 (scale bar, 50 μm). Immunohistochemistry and immunofluorescence staining were performed on a sample size of $n = 10$. **h** Distribution of TCRβ clonotypes by tr-TIL samples from 10 glioma patients. TCRβ chain frequencies are expressed as a percentage, with 2% as the lower cut-off value, and are shown in a Stacked Barplot generated using R 4.2.3 (URL: https://www.R-project.org/). The absolute count of TCR clonotypes is indicated above each barplot.
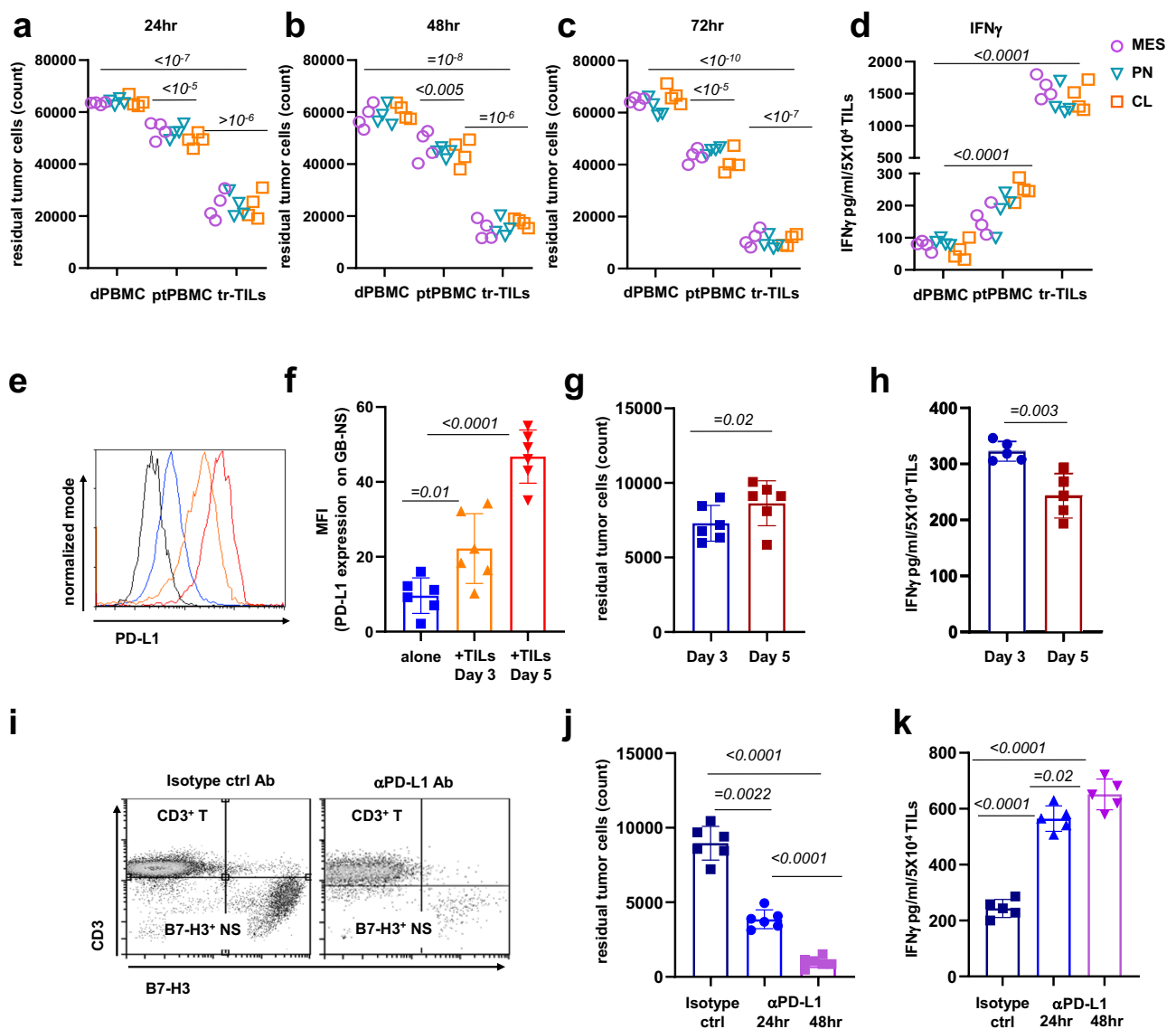
Fig. 4 | Tumor-reactive TILs exhibit specific antitumor activity against autologous tumor cells. a–h tr-TILs co-cultured with matched GB-NS. **a–c** Scatters plots showing the residual number of tumor cells (count) from different GB molecular subtypes when in co-culture with autologous tr-TILs or PBMCs (ptPBMC), and healthy donor PBMCs (dPBMC) at (**a**) 24, (**b**) 48, and (**c**) 72 h, at E: T ratio = 3:1. **d** Quantification of IFNγ (pg/ml) secreted by tr-TILs co-cultured with autologous tumor cells from different GB molecular subtypes (24 h); as controls dPBMC and ptPBMCs were used. Data were derived from 12 cases, 4 with mesenchymal, 4 with proneural and 4 with classical subtype. Data are presented as mean ± SD, with 2 technical replicates averaged prior to statistical analysis assessed using a two-tailed unpaired t test. **e** Representative flow cytometry histograms showing PD-L1 expression levels of GB-NS in co-culture with tr-TILs (orange: TILs + GB-NS Day 3; red: TILs + GB-NS Day 5) compared to FMO (fluorescence minus one) control (black) and GB-NS alone (blue). **f** Bar histograms showing PD-L1 MFI of GB-NS alone and in co-culture with tr-TILs (n = 6). Data are presented as mean ± SD and statistical significance was assessed using a two-tailed unpaired t test. **g** Scatter plot

showing residual tumor cells (count) in co-culture with tr-TILs at Day 3 and Day 5 (n = 6). Data are presented as mean ± SD, and statistical significance was assessed using a two-tailed unpaired t test. **h** ELISA quantification of IFNγ secreted by tr-TILs co-cultured with GB-NS at Day 3 and Day 5 (n = 5). Data are presented as mean ± SD, and statistical significance was assessed using a two-tailed unpaired t test. (**i–k**) PD-L1 blocking in tr-TILs co-cultured with GB-NS. **i** Representative flow cytometry plot of tr-TILs co-cultured with GB-NS in the presence of αPD-L1 antibody and in the presence of the isotype control (IgG2a/eBM2a). **j** Scatter plot showing the residual number of tumor cells (count) in co-culture with tr-TILs in the presence of αPD-L1 antibody and isotype control (IgG2a/eBM2a) at 24 and 48 h (n = 6). **k** ELISA quantification of IFNγ secreted by tr-TILs co-cultured with GB-NS in the presence of αPD-L1 antibody and isotype control at 24 and 48 h (n = 5). Data are presented as mean ± SD, and statistical significance was assessed using a two-tailed unpaired t test. Full numerical data and comprehensive details of statistical analyses are available in the corresponding source data tables for each figure. Source Data are provided as a Source Data file.

of the oncometabolite 2-hydroxyglutarate (2HG) in reducing the expression of *STAT-1*, limiting CXCL9 and CXCL10 production[34] and generally reshaping the tumor microenvironment[35].

We also analyzed the potential impact of steroid treatment on TIL expansion outcomes.

We collected information about steroid therapies and doses before surgery, when available, observing that the mean cumulative

dosage and treatment duration were significantly higher in not expanded samples compared to expanded samples. A threshold of 22 days was identified, beyond which negative expansion outcomes were likely (ROC curves). Additionally, a trend was observed indicating that newly diagnosed patients received greater and longer pre-operative steroid treatment compared to recurrent cases, although no significant differences in expansion outcomes were noted. In terms
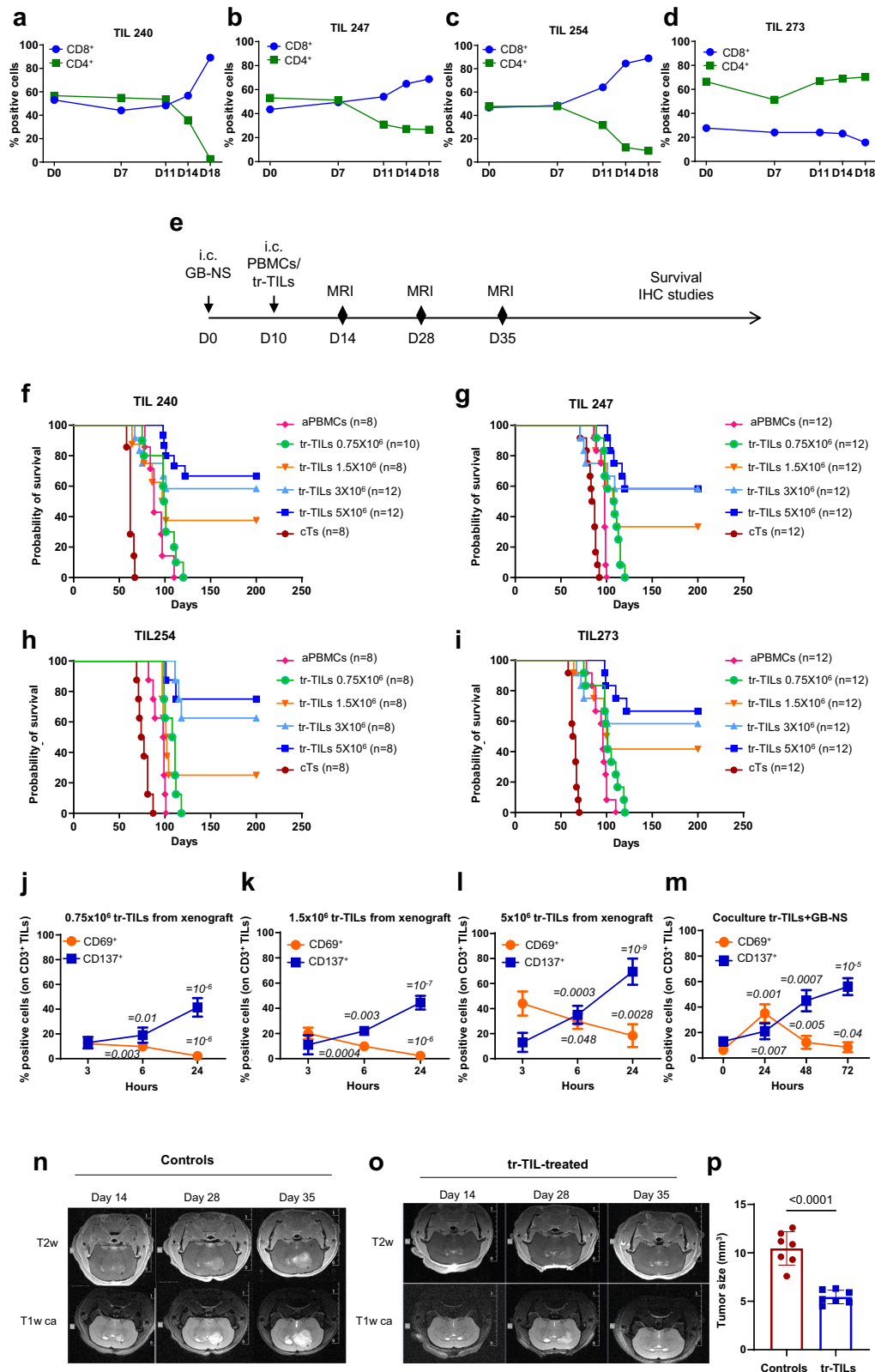
of immune infiltration, evidence indicates that steroid treatment may adversely affect the infiltration and functionality of dendritic cells[36] and may impair peripheral blood immune cell migration and redistribution within tumor tissue, although data on their functionality remains lacking[37]. However, high-dose steroids have been hypothesized to impair TIL antitumor activity and could diminish the efficacy of the TIL therapy. Elevated TIM-3 expression in CD4^{+}

TILs of not expanded samples was attributed to prolonged steroid exposure. Although increased TIM-3 is linked to remission in autoimmune diseases, in cancer it may signify terminal T cell exhaustion[38]. Understanding the difficulty in producing TILs, including the source and the quality of surgical material, quality of starting materials, inter-patient product heterogeneity, and difficulty in characterizing TILs, provided details of the tools should be used to

Fig. 5 | Tumor-reactive TILs control tumor growth in xenograft models.
a–d Frequency of CD4+ and CD8+ T cells of 4 tr-TILs samples during in vitro expansion. **e** Experimental schema of in vivo studies. **f–i** Kaplan Meier curves showing survival of nude mice treated with a dose escalation of tr-TILs. Four different TILs were tested (TIL 240, TIL 247, TIL 254, TIL 273). Control mice were treated with PBMCs or left untreated (control TILs - cTs). Comparisons between groups were performed using the log-rank (Mantel−Cox) test. **j–l** Expression of the activation markers CD69 and CD137 on tr-TILs isolated and analyzed 3, 6, and 24 h after intracranial injection of 0.75×10^6 (**j**), 1.5×10^6 (**k**), and 5×10^6 (**l**) in xenograft models. Data are presented as mean ± SD from 5 mice per group ($n = 5$), and statistical significance was assessed using a two-tailed paired t test. **m** Expression of

the activation markers CD69 and CD137 on tr-TILs ($n = 4$) during in vitro co-cultures at 24, 48, and 72 h. Data are presented as mean ± SD, and statistical significance was assessed using a two-tailed paired t test. **n, o** Representative MRI performed with T2-weighted images (T2-wi) and T1-weighted images (T1-wi) with contrast agent (ca) (**n**) on control and (**o**) TIL-treated xenograft mice; a total of 12 mice/condition were studied. **p** Bar graph showing the tumor volume measured using MRI and expressed as mm³ (controls vs TIL-treated mice). Data are presented as mean ± SD from 7 mice per group ($n = 7$) and statistical significance was assessed using a two-tailed unpaired t test. Full numerical data and comprehensive details of statistical analyses are available in the corresponding source data tables for each figure. Source Data are provided as a Source Data file.
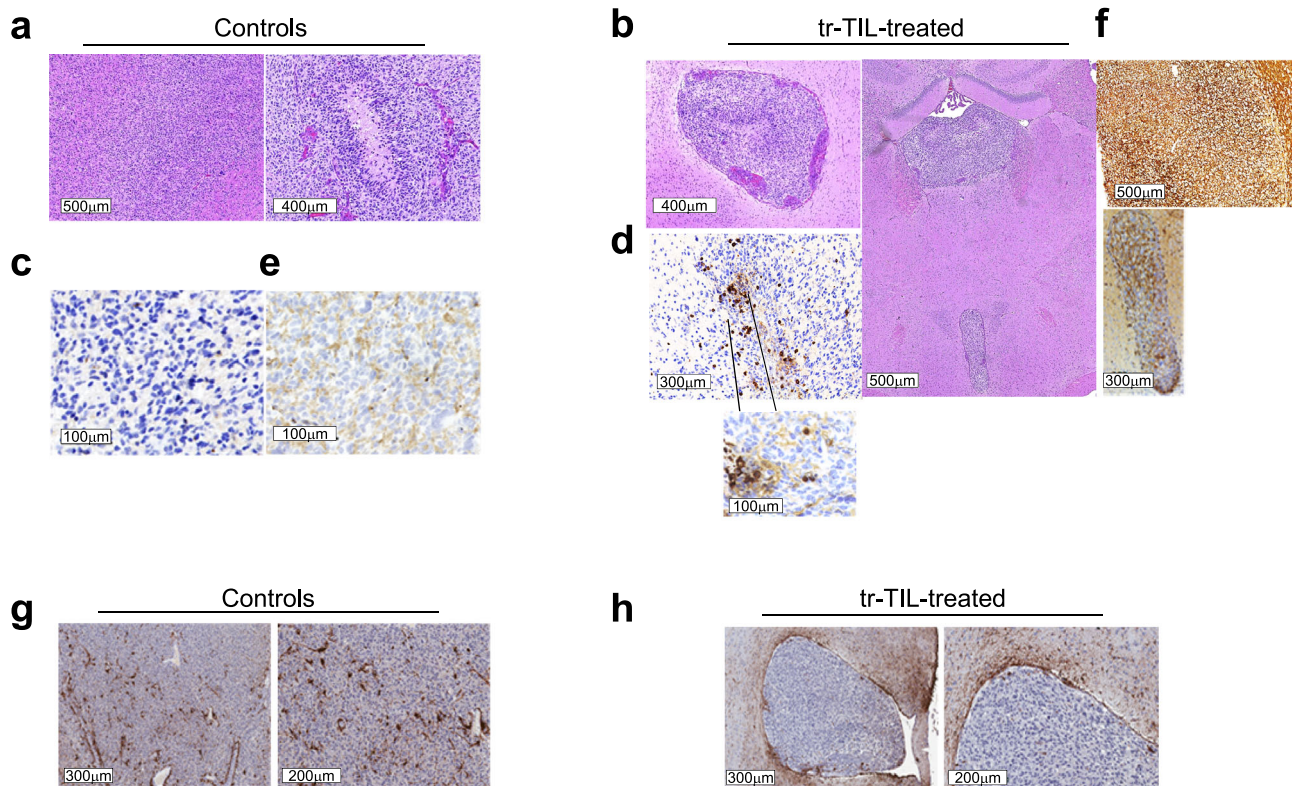
Fig. 6 | Persistence of CD8+ TILs and PD-L1 overexpression on tumor cells are found in xenograft gliomas. a, b Representative Hematoxylin&Eosin staining images showing the morphological characteristics of (**a**) tumors from control ($n = 7$) and (**b**) TIL-treated ($n = 7$) mice 60 days after tumor cell implantation (Scale bar, 500 and 400 µm); **c, d** anti-human CD3 staining performed on tumors revealed the presence of TILs in treated but not control mice (Scale bar, 300 and 100 µm,

respectively); (**d** inset) TILs persisting within the tumor mass were positive for CD8 (Scale bar, 100 µm). **e, f** PD-L1 staining of tumors (**e**) from control and (**f**) TIL-treated mice 60 days after tumor cell implantation (Scale bar, 100 and 500–300 µm, respectively). **g, h** Anti-human GFAP staining showing (**h**) a barrier surrounding tumor masses in treated mice (Scale bar 300 and 200 µm).

correctly achieve GMP transition. Our ability to produce a larger number of TILs using a rapid expansion protocol[39] strengthens its applicability and ability to be used in the clinic. Furthermore, we observed a (poly)clonal expansion of tr-TILs, including those isolated from recurrent glioblastomas. This suggests that polyclonal TIL populations may include multiple clonotypes with diverse TCR specificities, thereby potentially enabling them to address tumor antigen heterogeneity and enhance their therapeutic efficacy[40].

All the results and the use of a clinical-scale procedure providing a wider margin of safety encouraged us to incorporate this process into a forthcoming first in human clinical trial protocol, named ReacTIL.

Methods
Population and patient characteristics
A total of 161 patients underwent brain tumor removal using the CUSA after providing written informed consent regarding the collection, storage, and use of biological material for scientific analyses. The

study, included in a project funded by AIRC (IG22980), has been approved by the Fondazione IRCCS Istituto Neurologico Carlo Besta (FINCB) Ethics Committee. There were no restrictions on patient selection, and no biases related to sex or gender were present. At FINCB Institute, the neurosurgeons adhere to the surgical principle of maximizing tumor resection while minimizing the risk of inducing new neurological deficits. This strategy aims to strike an optimal balance between comprehensive tumor removal and preservation of neurological function.

The histological analysis revealed the following diagnoses: 138 IDH1 wild-type (110 newly diagnosed and 28 recurrent glioblastoma), and 23 IDH1-mutant (14 astrocytoma, including 5 grade 4, 8 grade 3, 1 grade 2; 6 oligodendroglioma, including 4 grades 3 and 2 grade 2; and 3 recurrent glioblastomas, including 2 grades 4 and 1 grade 3). Clinical data, including age, sex, steroid dosage and duration, tumor site, IDH1 status, and MGMT status, were collected and are reported in Table 1 and Supplementary Data 1. MGMT promoter methylation

status was assessed by methylation-specific polymerase chain reaction using specific primers[41]. IDH1 gene mutation detection was performed using primer pairs specific for exon 4 and determined by Sanger sequencing (Applied Biosystems 3500 and 3500 Dx Series Genetic Analyzer).

Tumor dissociation, isolation, and expansion of tr-TILs

CUSA material containing tumor fragments was transferred to 50 ml tubes and centrifuged. Necrotic or coagulated parts were removed from the suspension. Tumor fragments were washed with HBSS plus DNase I (Merck), diluted with collagenase type I (Merck), and digested using GentleMACS Octo Dissociator (Miltenyi Biotec). After digestion, an aliquot of the cell suspension was seeded to derive primary tumor cells[21]. Cell debris was removed from the rest of the cell suspension with Debris Removal Solution (Miltenyi Biotec) according to the manufacturer's instructions. This density gradient reagent also efficiently removes tumor cells, which remain at the interface along with the cell debris after centrifugation, while the pellet containing immune cells can be easily isolated. The pellet containing immune cells was treated with ACK solution (ThermoFisher Scientific) to obtain red blood cell lysates, after which the cells were counted and analyzed for viability and the percentage of CD137+. Tumor reactive (tr-)TILs were enriched by using the CD137 MicroBead Kit (Miltenyi Biotec). Donor-derived and matched peripheral blood mononuclear cells (PBMCs) were isolated from peripheral blood. Tr-TILs and PBMCs were seeded at a concentration of 0.5×10^5/well) in TexMACS GMP Medium (Miltenyi Biotec) supplemented with 30 ng/ml OKT3 (MACS® GMP CD3 Pure, Miltenyi Biotec), 3% human serum, IL-15, IL-7 and IL-21 (10 ng/ml, GMP PeproTech) and irradiated allogeneic feeder cells (TILs/PBMC: feeder=1:50). TILs and PBMCs were cultured in 24-well plates at 37 ± 1 °C and 5 ± 1% CO2 for 6 ± 1 days. After this time, the TILs were transferred to a T25 vent cap flask at a final volume of 8 mL until Day 12. On Day 12, the medium volume was doubled. After 14 days, the TILs were collected, analyzed for viability and immunophenotyping, and transferred to a T75 flask at a concentration of 0.2×10^6 cells/ml. After that, the cells were expanded without any further addition of OKT3 or feeder cells for 18 days.

Depending on cell recovery, a portion of the cell was subjected to a second round of rapid expansion starting from frozen samples. tr-TILs were expanded for two weeks (14 days) following the same expansion protocol used at day 0 (i.e., OKT3 and feeder in the presence of IL-15, IL-7 and IL-21) and characterized by immunophenotype.

Expansion of glioblastoma neurospheres (GB-NS)

Primary tumor cells were cultured as neurospheres (NS) in DMEM-F12 Glutamax (Thermofisher Scientific) supplemented with B27 supplement (Thermofisher Scientific, Catalog no.17504044), human recombinant EGF (20 ng/ml, Peprotech, Catalog no. 17504044) and b-FGF (20 ng/ml, PeproTech, Catalog no. 100-18B). At each passage, NS were mechanically dissociated into a single suspension, and an aliquot frozen when possible. NS were always used between passages 8 and 12 for co-culture assay and downstream applications. All the primary cell lines are stored in the Besta Brain Tumor Biobank, managed by SOL Group Spa (Italy).

Immunophenotyping

The immunophenotyping of the manufactured tr-TILs was performed to confirm the cell composition of the product. The cells were incubated at RT for 10 minutes in the presence of REA antibodies (Miltenyi Biotec) conjugated with fluorochromes, acquired with a MACSQuant Analyzer 16 (Miltenyi Biotec) and analyzed with FlowJo software. Before acquisition, 7-AAD (Miltenyi Biotec) was added to exclude dead cells. The results for each marker are expressed as the percentage of cells among the total viable CD45-positive cells.

The following markers were used to define. Memory phenotype: CD45RA Antibody, anti-human, VioBlue®, REAfinity™, Clone REA562, Catalog no. 130-120-033; CD4 Antibody, anti-human, VioGreen™, REAfinity™, Clone REA623, Catalog no. 130-113-230; CD3 Antibody, anti-human, FITC, REAfinity™, Clone REA613, Catalog no. 130-113-138; CD197 (CCR7) Antibody, anti-human, PE, REAfinity™, Clone REA108, Catalog no. 130-120-463; CD62L Antibody, anti-human, PE-Vio® 770, REAfinity™, Clone REA615, Catalog no. 130-129-810; CD45RO Antibody, anti-human, APC, REAfinity™, Clone REA611, Catalog no. 130-113-556; CD8 Antibody, anti-human, APC-Vio® 770, REAfinity™, Clone REA734, Catalog no. 130-110-681; 7-AAD Staining Solution, Catalog no. 130-111-568.

Exhaustion phenotype: CD223 Antibody, anti-human, VioBlue®, REAfinity™, Clone REA351, Catalog no. 130-118-549; CD4 Antibody, anti-human, VioGreen™, REAfinity™, Clone REA623, Catalog no. 130-113-230; CD3 Antibody, anti-human, FITC, REAfinity™, Clone REA613, Catalog no. 130-113-138; CD137 Antibody, anti-human, PE, REAfinity™, Clone REA765, Catalog no. 130-110-763; CD279 (PD-1) Antibody, anti-human, PE-Vio® 770, REAfinity™, Clone REA1165; Catalog no. 130-120-385; CD366 (TIM-3) Antibody, anti-human, APC, REAfinity™, Clone REA635, Catalog no. 130-119-781; CD8 Antibody, anti-human, APC-Vio® 770, REAfinity™, Clone REA734, Catalog no. 130-110-681; 7-AAD Staining Solution, Catalog no. 130-111-568.

CD137 enrichment: CD45 Antibody, anti-human, VioBlue®, REAfinity™, Clone REA747, Catalog no. 130-110-637; CD3 Antibody, anti-human, APC, REAfinity™, Clone REA613, Catalog no. 130-113-135; CD8 Antibody, anti-human, PE-Vio® 770, REAfinity™, Clone REA734, Catalog no. 130-110-680; CD4 Antibody, anti-human, Vio® Bright FITC, REAfinity™, Clone REA623, Catalog no. 130-113-229; CD137 Antibody, anti-human, PE, REAfinity™, Clone REA765, Catalog no. 130-110-763; 7-AAD Staining Solution, Catalog no. 130-111-568.

Mouse blood samples: CD45 Antibody, anti-human, VioBlue®, REAfinity™, Clone REA747, Catalog no. 130-110-637; CD3 Antibody, anti-human, APC, REAfinity™, Clone REA613, Catalog no. 130-113-135;

CD137 Enrichment: Magnetic sorting selection: CD137 MicroBead Kit human, Catalog no. 130-093-476, containing CD137-PE, human monoclonal CD137 antibody conjugated to PE (isotype: mouse IgG1) and Anti-PE MicroBeads: MicroBeads conjugated to monoclonal anti-PE antibodies. Assessment of tr-TIL enrichment: CD45 Antibody, anti-human, VioBlue®, REAfinity™, Clone REA747, Catalog no. 130-110-637; CD3 Antibody, anti-human, APC, REAfinity™, Clone REA613, Catalog no. 130-113-135; CD8 Antibody, anti-human, PE-Vio® 770, REAfinity™, Clone REA734, Catalog no. 130-110-680; CD4 Antibody, anti-human, Vio® Bright FITC, REAfinity™, Clone REA623, Catalog no. 130-113-229; CD137 Antibody, anti-human, PE, REAfinity™, Clone REA765, Catalog no. 130-110-763; 7-AAD Staining Solution, Catalog no. 130-111-568.

Co-colture tr-TILs - GB NS: CD3 Antibody, anti-human, FITC, REAfinity™, Clone REA613, Catalog no. 130-113-138; CD4 Antibody, anti-human, VioGreen™, REAfinity™, Clone REA623, Catalog no. 130-113-230; CD8 Antibody, anti-human, APC-Vio® 770, REAfinity™, Clone REA734, Catalog no. 130-110-681; CD276 (B7-H3) Antibody, anti-human, PE, REAfinity™, Clone REA1094, Catalog no. 130-118-570; CD274 (B7-H1/PD-L1) Antibody, anti-human, Vio® Bright R720, REAfinity™, Clone REA1197, Catalog no. 130-131-660; 7-AAD Staining Solution, Catalog no. 130-111-568.

TCRVβ sequencing

T cell diversity and clonal expansion were tested by sequencing T cell receptor (TCR) beta chain rearrangements using AmpliSeq for Illumina TCR beta-SR Panel that amplifies the CDR3 region of the *TCRb* gene, according to the manufacturer's instructions. A total of 10 ng input RNA isolated from 10 TIL samples was used. The extraction was performed using TRIzol (ThermoFisher Scientific) combined with QIAGEN spin-column technology. The quality of TCR libraries was assessed using Bioanalyzer2100-High Sensitivity DNA kit (Agilent) and Qubit Fluorometric – Qubit dsDNA HS Assay kit (ThermoFisher Scientific).

The library preparation was followed by paired-end sequencing on a NextSeq 550 platform using Mid Output Flow Cell Cartrige v2.5 (300 cycles, 2 × 150 reads). TCRSeq data in FASTQ format were pre-processed with MiXCR Immune Repertoire Analyzer software (v4.7.0)[42] for read alignment and clonotype assembly. Subsequently, clones with less than 2% frequency were filtered out, calculating the TCRβ chain frequency as a percentage based on read counts.

Killing assay and ELISA assay

Co-culture assays were performed by plating matched glioblastoma neurospheres (GB-NS) with TILs or PBMCs (either donor-derived or matched PBMCs) at an E:T ratio of 3:1 in GB-NS medium without serum and in the presence of B27 supplement (Gibco)[21,43]. PD-L1 blocking was performed with αPD-L1 antibody (10 μg/ml; Monoclonal Antibody (MIH1), Functional Grade, eBioscience Catalog no. 16-5983-82, from ThermoFisher Scientific) or isotype control (10 μg/ml; IgG2a/eBM2a antibody functional Grade, eBioscience; Catalog no 16-4724-82, from ThermoFisher Scientific). GB-NS and T cells were collected at different time points (24, 48 and 72 h), and residual tumor cells and T cells were measured by flow cytometry based on B7-H3[17] and CD3 expression, respectively. The absolute cell count is obtained by volumetric measurement with a precision volume uptake syringe on the MACSQuant® Analyzer16 (Miltenyi Biotec). Co-culture supernatants were collected after 24 h to measure IFNγ using a specific ELISA (Catalog #: DY285B; R&D Systems, Minneapolis, MN).

Real-time PCR

Total RNA from TIL samples at different time points during expansion was extracted using TRIzol (Life Technologies) and reverse-transcribed using a high-capacity cDNA synthesis kit (ThermoFisher Scientific). The expression of genes was analyzed by real-time PCR with the SYBR Green method (Fast SYBR™ Green Master Mix, ThermoFisher Scientific). RNA from baseline PBMC samples (ThermoFisher Scientific) was used as a calibrator for the calculation of fold changes in expression levels via the ΔΔCt method. The expression levels of target genes were normalized to the expression level of β2 microglobulin.

Oligonucleotides sequences. *TCF7*: (FW) AAAAGCACCAA-GAATCCACCAC; (RV) AGCACTGTCATCGGAAGGAA

PDCD1: (FW) TGGACTATGGGGAGCTGGATT; (RV) ACAATGGTGG CATACTCCGTC

GZMK: (FW) TGAGGCCTCCAAACAAACAC; (RV) TGAGTTTTGCGG CTGTTTGA

SELL: (FW) GCATTCTCTGGGTTGGCATTT; (RV) TTCTTTCACC AAGGGCGATT

IFNG: (FW) CATCCAAGTGATGGCTGAAC; (RV) CTTCGACCTCG AAACAGCAT

HAVCR2: (FW) GTCATCAAACCAGCCAAGGTC; (RV) CCATGTCCC CTGGTGGTAAG

β2M: (FW) ACTGAATTCACCCCCACTGA; (RV) CCTCCATGATG CTGCTTACA

Animal studies

All animal manipulations were performed following the directives of Fondazione IRCCS Istituto Neurologico Carlo Besta in Milan in accordance with the Italian Principle of Laboratory Animal Care (D. Lgs. 26/2014) and authorized by Ministry of Health (prot. 2A349.27). Six-week-old female nude mice (Crl:CD1-Foxn1nu) were injected i.c. with 1 × 10^5 primary tumor cells in 2 μL of PBS. The coordinates, with respect to the bregma, were 0.7 mm post, 3 mm left lateral, and 3.5 mm deep within the *nucleus caudatum*. On Day 10 after tumor cell implantation, a dose escalation study was performed by injecting four doses of tr-TILs from 5×10^6 to 0.75×10^6. tr-TILs were injected i.c. in 5 μL of PBS using the same tumor coordinates. Matched PBMC were administrated as control (5×10^6). Blood samples were collected for one week from untreated, PBMC treated and 5×10^6 tr-TIL treated mice, stained with anti-human CD45 and CD3 Abs and analyzed by flow cytometry after erythrocyte lysis using RBC Lysis Buffer (ThermoFisher Scientific). For survival studies, mice were monitored and euthanized when signs of discomfort appeared in accordance with the institutional guidelines. Brains were collected and used to isolate tumor material from fresh samples or fixed in 4% paraformaldehyde for histological studies.

Only female mice were used for this study, as it was not designed to detect sex differences.

Magnetic resonance imaging (MRI)

In vivo MRI experiments were performed by a horizontal-bore pre-clinical scanner (7 Tesla, BioSpec 70/20 USR, Bruker, Ettlingen, Germany). Mice were anesthetized with 1.5–2% isoflurane (60:40 N2O:O2 (vol: vol), flow rate 0.8 L/min). To detect the depth of anesthesia and the animal health condition during the study, the respiratory rate was monitored by a pneumatic sensor. Mice injected with GB-NS and treated with TILs underwent high-resolution MRI at different time points with the following protocol: a T2-weighted Rapid Acquisition with Reduced Echoes (RARE) sequence (TR = 3360 ms, TE = 35 ms, in plane resolution = 100 × 100 μm2, slice thickness = 400 μm, 4 averages, total acquisition time of 5 min 36 sec) and two T1-weighted RARE sequences (TR = 510 ms, TE = 8 ms, in plane resolution = 78 × 78 μm2, slice thickness = 400 μm, 6 averages, total acquisition time of 9 min 47 sec) acquired before and after intraperitoneal administration of Gadoliunium-based contrast medium.

Tumor size quantification

Tumor volume was calculated from T2-weighted MRI images using a semi-automatic segmentation algorithm. The method initially identifies hyperintense tumor voxels based on a whole-brain signal intensity threshold. Two operators (including a clinical radiologist) then select a point within the tumor, from which only the voxels belonging to the tumor are isolated in 3D using morphological operators. This step is followed by manual refinements to correct any areas where the automated segmentation either missed portions of the tumor or included non-tumor regions. This two-step process ensures greater precision in segmentation. The total tumor volume was then estimated by summing the number of selected voxels and multiplying by the voxel size of the corresponding T2w sequence, allowing for a reliable volumetric assessment of the tumor (mm^3).

Immunohistochemistry (IHC)

For immunohistological (IHC) analyses, human brain tumor and xenograft samples were sliced in 2–4 μm thick sections, and the process was performed on an automated staining Leica Bond MAX system using Epitope Retrieval solution 2 (ER2, pH 9) for 20 minutes at 98 °C and BOND Polymer refine Detection System DAB (Leica Microsystems). Slides were counterstained with hematoxylin (Sigma-Aldrich), dehydrated, and mounted. The expression of all antibodies was evaluated for intensity of reactivity and tissue localization. Briefly, mouse tissue slides were incubated with anti-human CD3 mouse monoclonal antibody (1:50, Mouse monoclonal anti-human CD3 clone F7.2.38 M7254 DAKO) for 20 minutes, with PD-L1 antibody (1:100, Mouse monoclonal anti-human PD-L1 clone 22C3 M3653 DAKO) for 1 h at room temperature, with anti-human CD8 mouse monoclonal antibody (1:50, Mouse monoclonal anti-human CD8 clone C8/1448 M7103 DAKO) for 20 minutes and anti-GFAP antibody (1:12000, Mouse monoclonal anti-glial Fibrillary Acidic Protein Clone GA5 Sigma Aldrich USA) for 30 minutes.

For double immunohistochemistry, following incubation with biotinylated antibody anti-CD137 (1:2, CliniMACS CD137-biotin #170-076-707 Miltenyi Biotec) and detection using streptavidin-HRP and DAB chromogen, human tissue sections (2 μm) were processed on the BOND-III system (Leica Biosystems) using the BOND Polymer Refine Red Detection kit (DS9390). After dewaxing, the slides were incubated

with the primary antibody anti-CD8 for 60 minutes. Detection was performed using an alkaline phosphatase polymer and Fast Red chromogen. Slides were counterstained with hematoxylin, then dehydrated through a graded alcohol series (70% to absolute ethanol) followed by xylene and mounted with Eukitt. IHC slide scanning was performed using an Aperio CS2 - Digital Pathology Slide Scanner. Qualitative analyses of CD8 and TCF1 expression were blindly performed by three independent investigators on five independent fields per tumor in the photographed fields using the 20× and 40× objectives of a Zeiss LSM980-Airyscan. To identify the distribution of CD8 staining, a heat map was generated for each immunohistochemistry image using Qupath software in a pixel-based analysis. We generated a density map that visualized stain intensity and the location of positive cells within immune cell annotation.

Immunofluorescence (IF)
For immunofluorescence (IF) analyses, human tissue slides were incubated with anti-CD8 mouse monoclonal antibody (1:50, Mouse monoclonal anti-human CD8 clone C8/1448 M7103 DAKO) for 20 minutes at room temperature. A double immunofluorescence staining with the anti–human TCF1 polyclonal antibody (1:50, Anti-TCF1, goat anti-human, cod. AF5596 R&D Systems, Minneapolis, MN) and the same anti-CD8 antibody (1:25) was performed. Donkey anti-mouse Alexa-568 antibody (red, 1:200) and donkey anti-goat Alexa-488 (green, 1:400) were used to detect CD8 and TCF1, respectively. Cell nuclei were counterstained with DAPI (Sigma-Aldrich), and the slides were mounted with a PBS/glycerol solution.

Single-cell multiplexed secretome proteomics (IsoPlex)
Tr-TILs were seeded and stimulated with anti-CD3 and CD28 at 37 °C for 24 h. Both stimulated and unstimulated TILs were collected, stained, and processed using IsoPlex's automated system. Chips were imaged for cell detection, followed by ELISA protocol execution and signal imaging. Raw data images were inputted, and cell detection, signal detection, and alignment were performed automatically. An interactive analysis facilitated the comparison of raw data between samples. The polyfunctional profile (defined as >2 cytokines secreted per cell) of individual cells was assessed, generating a polyfunctional strength index (PSI) score, with further classification into effector, stimulatory, chemoattraction, regulatory, and inflammatory categories.

Statistical analyses
Descriptive statistics (i.e., means, medians, standard deviations and/or percentages/frequencies) are reported for all markers; in particular, in vitro and in vivo data are presented as the means ± standard deviations (SDs). The chi-square test or Fisher's exact test was used to evaluate the differences in categorical variables between the expanded subgroup and the not expanded subgroup, with a p value < 0.05 considered to indicate statistical significance. The following categorical variables were considered: the presence of IDH1 mutation or MGMT methylation status in tumor samples, sex, age (<=45 vs. >45; <=65 vs.>65), and steroid presence or treatment duration. The cutoff value of steroid treatment duration was defined using ROC curve analysis. The Wilcoxon-Mann-Whitney test was used to test the significance of differences between markers. All p values were two-sided. Changes from baseline were analyzed through ANOVA or a corresponding nonparametric analysis. Kaplan-Meier analysis was used to estimate overall survival. All the statistical analyses were performed using GraphPad Prism 10.1.2 software.

The study was approved by the Ethics Committee, and it is in accordance with the Helsinki Declaration.

Reporting summary
Further information on research design is available in the Nature Portfolio Reporting Summary linked to this article.

Data availability

References
1. Stupp, R. et al. Radiotherapy plus concomitant and adjuvant temozolomide for glioblastoma. *N. Engl. J. Med.* **352**, 987–996 (2005).
2. Betof Warner, A., Corrie, P. G. & Hamid, O. Tumor-infiltrating lymphocyte therapy in melanoma: facts to the future. *Clin. Cancer Res.* **29**, 1835–1854 (2023).
3. Mullard, A. Tumour-infiltrating lymphocyte cancer therapy nears FDA finish line. *Nat. Rev. Drug Discov.* **23**, 3–7 (2024).
4. Oliveira, G. & Wu, C. J. Dynamics and specificities of T cells in cancer immunotherapy. *Nat. Rev. Cancer* **23**, 295–316 (2023).
5. Johanns, T. M. et al. Immunogenomics of hypermutated glioblastoma: a patient with germline pole deficiency treated with checkpoint blockade immunotherapy. *Cancer Discov.* **6**, 1230–1236 (2016).
6. Cloughesy, T. F. et al. Neoadjuvant anti-PD-1 immunotherapy promotes a survival benefit with intratumoral and systemic immune responses in recurrent glioblastoma. *Nat. Med.* **25**, 477–486 (2019).
7. Anghileri, E. et al. High tumor mutational burden and T-cell activation are associated with long-term response to anti-PD1 therapy in Lynch syndrome recurrent glioblastoma patient. *Cancer Immunol. Immunother.* **70**, 831–842 (2021).
8. Hudson, W. H. & Wieland, A. Technology meets TILs: deciphering T cell function in the -omics era. *Cancer Cell* **41**, 41–57 (2023).
9. Kaminska, B., Ochocka, N. & Segit, P. Single-cell omics in dissecting immune microenvironment of malignant gliomas-challenges and perspectives. *Cells* **10**, 2264 (2021).
10. Hoogstrate, Y. et al. Transcriptome analysis reveals tumor microenvironment changes in glioblastoma. *Cancer Cell* **41**, 678–692.e7 (2023).
11. Ravi, V. M. et al. Spatially resolved multi-omics deciphers bidirectional tumor-host interdependence in glioblastoma. *Cancer Cell* **40**, 639–655.e13 (2022).
12. Sattiraju, A. et al. Hypoxic niches attract and sequester tumor-associated macrophages and cytotoxic T cells and reprogram them for immunosuppression. *Immunity* **56**, 1825–1843.e6 (2023).
13. Musca, B. et al. The immune cell landscape of glioblastoma patients highlights a myeloid-enriched and immune suppressed microenvironment compared to metastatic brain tumors. *Front. Immunol.* **14**, 1236824 (2023).
14. Wang, A. Z. et al. Glioblastoma-infiltrating CD8 + T cells are predominantly a clonally expanded GZMK+ effector population. *Cancer Discov.* **14**, 1106–1131 (2024).
15. Ye, Q. et al. CD137 accurately identifies and enriches for naturally occurring tumor-reactive T cells in tumor. *Clin. Cancer Res.* **20**, 44–55 (2014).
16. Seliktar-Ofir, S. et al. Selection of shared and neoantigen-reactive T cells for adoptive cell therapy based on CD137 separation. *Front. Immunol.* **8**, 1211 (2017).
17. Nehama, D. et al. B7-H3-redirected chimeric antigen receptor T cells target glioblastoma and neurospheres. *EbioMedicine* **47**, 33–43 (2019).
18. Mullard, A. FDA approves first tumour-infiltrating lymphocyte (TIL) therapy, bolstering hopes for cell therapies in solid cancers. *Nat. Rev. Drug Discov.* **23**, 238 (2024).
19. Wang, L. et al. A single-cell atlas of glioblastoma evolution under therapy reveals cell-intrinsic and cell-extrinsic therapeutic targets. *Nat. Cancer* **3**, 1534–1552 (2022).

20. Schmassmann, P. et al. Single-cell characterization of human GBM reveals regional differences in tumor-infiltrating leukocyte activation. *eLife* **12**, RP92678 (2023).

21. Finocchiaro, G. & Pellegatta, S. Immunotherapy with dendritic cells loaded with glioblastoma stem cells: from preclinical to clinical studies. *Cancer Immunol. Immunother.* **65**, 101–109 (2016).

22. Day, B. W. et al. Glioma surgical aspirate: a viable source of tumor tissue for experimental research. *Cancers (Basel)* **5**, 357–371 (2013).

23. Yang, G. et al. Functional status and spatial architecture of tumor-infiltrating CD8 + T cells are associated with lymph node metastases in non-small cell lung cancer. *J. Transl. Med.* **21**, 320 (2023).

24. Mann, T. H. & Kaech, S. M. Tick-TOX, it's time for T cell exhaustion. *Nat. Immunol.* **20**, 1092–1094 (2019).

25. Drenkard, D. et al. CD137 is expressed on blood vessel walls at sites of inflammation and enhances monocyte migratory activity. *FASEB J.* **21**, 456–463 (2007).

26. Glorieux, C. & Huang, P. CD137 expression in cancer cells: regulation and significance. *Cancer Commun. (Lond.)* **39**, 70 (2019).

27. Glorieux, C. & Huang, P. Regulation of CD137 expression through K-Ras signaling in pancreatic cancer cells. *Cancer Commun. (Lond.)* **39**, 41 (2019).

28. Watowich, M. B., Gilbert, M. R. & Larion, M. T cell exhaustion in malignant gliomas. *Trends Cancer* **9**, 270–292 (2023).

29. Davidson, T. B. et al. Expression of PD-1 by T cells in malignant glioma patients reflects exhaustion and activation. *Clin. Cancer Res.* **25**, 1913–1922 (2019).

30. Lee, J. et al. IL-15 promotes self-renewal of progenitor exhausted CD8 T cells during persistent antigenic stimulation. *Front. Immunol.* **14**, 1117092 (2023).

31. Marton, C., Mercier-Letondal, P., Galaine, J. & Godet, Y. An unmet need: harmonization of IL-7 and IL-15 combination for the ex vivo generation of minimally differentiated T cells. *Cell. Immunol.* **363**, 104314 (2021).

32. Tooley, K. A., Escobar, G. & Anderson, A. C. Spatial determinants of CD8 + T cell differentiation in cancer. *Trends Cancer* **8**, 642–654 (2022).

33. Amankulor, N. M. et al. Mutant IDH1 regulates the tumor-associated immune system in gliomas. *Genes Dev.* **31**, 774–786 (2017).

34. Kohanbash, G. et al. Isocitrate dehydrogenase mutations suppress STAT1 and CD8+ T cell accumulation in gliomas. *J. Clin. Investig.* **127**, 1425–1437 (2017).

35. Bunse, L. et al. Suppression of antitumor T cell immunity by the oncometabolite (R)–2-hydroxyglutarate. *Nat. Med.* **24**, 1192–1203 (2018).

36. Carenza, C. Perioperative corticosteroid treatment impairs tumor-infiltrating dendritic cells in patients with newly diagnosed adult-type diffuse gliomas. *Front. Immunol.* **13**, 1074762 (2022).

37. Chitadze, G. In-depth immunophenotyping of patients with glioblastoma multiforme: Impact of steroid treatment. *Oncoimmunology* **6**, 11 (2017).

38. Schnell, A. Stem-like T cells in cancer and autoimmunity. *Immunol. Rev.* **325**, 9–22 (2024).

39. Betof Warner, A. et al. Expert consensus guidelines on management and best practices for tumor-infiltrating lymphocyte cell therapy. *J. Immunother. Cancer.* **12**, e008735 (2024).

40. Chiffelle, J. et al. Tumor-reactive T cell clonotype dynamics underlying clinical response to TIL therapy in melanoma. *Immunity* **57**, 2466–2482.e12 (2024).

41. Eoli, M. et al. Methylation of O6-methylguanine DNA methyltransferase and loss of heterozygosity on 19q and/or 17p are overlapping features of secondary glioblastomas with prolonged survival. *Clin. Cancer Res.* **13**, 2606–2613 (2007).

42. Bolotin, D. A. et al. MiXCR: software for comprehensive adaptive immunity profiling. *Nat. Methods* **12**, 380–381 (2015).

43. Behnan, J. et al. Ultrasonic surgical aspirate is a reliable source for culturing glioblastoma stem cells. *Sci. Rep.* **6**, 32788 (2016).

Acknowledgements

Author contributions

Conceptualization of the study: S.P., C.T., D.M.; Experimental design: M.M., S.M., N.D.I., C.T., D.M., S.P.; Conducting experiments and acquiring data: M.M., S.M., N.D.I., A.R., M.P., I.S., D.A., M.Z., Man.Fac., A.G., Mar.Far., P.C., F.Ag.; Surgery and follow up of the patients: L.M., F.Ac., F.DM.; Histological diagnosis: B.P.; Clinical information of the patients: M.E., A.S., G.B.; Genetic and molecular analysis: A.B., L.M., R.V., R.P.; Manuscript preparation: C.T., D.M., S.P.; Editing: M.E., C.T., D.M.

Competing interests

The authors declare no competing interests.

Additional information

Supplementary information The online version contains supplementary material available at https://doi.org/10.1038/s41467-025-62263-2.

Correspondence and requests for materials should be addressed to Serena Pellegatta.

Peer review information *Nature Communications* thanks Robert Prins and the other, anonymous, reviewer(s) for their contribution to the peer review of this work. A peer review file is available.

Reprints and permissions information is available at http://www.nature.com/reprints

[1]Unit of Immunotherapy of Brain Tumors, Fondazione IRCCS Istituto Neurologico Carlo Besta, Milan, Italy. [2]Unit of Neuroncology, Fondazione IRCCS Istituto Neurologico Carlo Besta, Milan, Italy. [3]Cell Factory, Fondazione IRCCS Policlinico San Matteo, Pavia, Italy. [4]Unit of Neuropathology, Fondazione IRCCS Istituto Neurologico Carlo Besta, Milan, Italy. [5]Data Science Unit, Fondazione IRCCS Istituto Neurologico Carlo Besta, Milan, Italy. [6]Laboratoy of Genetics Neuro-Oncology, Fondazione IRCCS Istituto Neurologico Carlo Besta, Milan, Italy. [7]Unit of Experimental Imaging, Fondazione IRCCS Istituto Neurologico Carlo Besta, Milan, Italy. [8]Department of Anesthesia, Intensive Care and Palliative Care, Fondazione IRCCS Istituto Nazionale dei Tumori, Milan, Italy. [9]Laboratory of Supramolecular and Bio-Nanomaterials, Politecnico di Milano, Milan, Italy. [10]Department of NeuroSurgery, Fondazione IRCCS Istituto Neurologico Carlo Besta, Milan, Italy. [11]Immunohematology and Transfusion Medicine Service, Fondazione IRCCS Istituto Nazionale dei Tumori, Milan, Italy. [12]Department of Translational Research and New Technologies in Medicine and Surgery, University of Pisa, Pisa, Italy. [13]Neurosurgery Unit, Pisa University Hospital, Pisa, Italy. [14]Department of Oncology and Hemato-oncology, University of Milan, Milan, Italy. [15]Department of Neurological Surgery, Johns Hopkins Medical School, Baltimore, MD, USA. [16]Unit of Molecular Neuro-Oncology, Fondazione IRCCS Istituto Neurologico Carlo Besta, Milan, Italy. [17]Unit of Cell Therapy Fondazione IRCCS Istituto Neurologico Carlo Besta, Milan, Italy. [18]Department of Sciences Clinic-Surgical, Diagnostic and Pediatric, University of Pavia, Pavia, Italy. [19]Pediatric Clinic, Fondazione IRCCS Policlinico San Matteo, Pavia, Italy. [20]These authors contributed equally: Martina Maffezzini, Silvia Musio, Natalia Di Ianni. [21]These authors jointly supervised this work: Catia Traversari, Daniela Montagna, Serena Pellegatta. ✉e-mail: serena.pellegatta@istituto-besta.it